THE JOURNAL OF PHYSICAL CHEMISTRY A

Article

pubs.acs.org/JPCA

Ab Initio Chemical Kinetics for $SiH_2 + Si_2H_6$ and $SiH_3 + Si_2H_5$ Reactions and the Related Unimolecular Decomposition of Si_3H_8 under a-Si/H CVD Conditions

P. Raghunath and M. C. Lin*

Center for Interdisciplinary Molecular Science, Department of Applied Chemistry, National Chiao Tung University, Hsinchu 300, Taiwan

Supporting Information

ABSTRACT: The kinetics and mechanisms for $SiH_2 + Si_2H_6$ and $SiH_3 + Si_2H_5$ reactions and the related unimolecular decomposition of Si_3H_8 have been investigated by ab initio molecular orbital theory based on the QCISD(T)/CBS//QCISD/6-311++G(d,p) method in conjunction with quantum statistical variational Rice−Ramsperger−Kassel−Marcus (RRKM) calculations. For the barrierless radical association processes, their variational transition states have been characterized by the CASPT2//CASSCF method. The species involved in the study are known to coexist under CVD conditions. The results show that the association reaction of SiH_2 and Si_2H_6 producing Si_3H_8 occurs by insertion via its lowest-energy path forming a loose hydrogen-bonding molecular complex with 8.3 kcal/mol binding energy; the reaction is exothermic by 55.0 kcal/mol. The chemically activated Si_3H_8 adduct can fragment by several paths, producing $SiH_4 + SiH_3SiH$ (−0.7 kcal/mol), $Si(SiH_3)_2 + H_2$ (−1.4 kcal/mol), and $SiH_3SiH_2SiH + H_2$ (−1.4 kcal/mol). The predicted enthalpy changes as given agree well with available thermochemical data. Three other decomposition channels of Si_3H_8 occurring by Si−H or Si−Si breaking were found to be highly endothermic, and the reactions take place without a well-defined barrier. The heats of formation of Si_3H_8, SiH_2SiH, Si_2H_4, *i*-Si_3H_7, *n*-Si_3H_7, $Si(SiH_3)_2$, and SiH_3SiH_2SiH have been predicted and found to be in close agreement with those available data in the literature. The product branching rate constants for $SiH_2 + Si_2H_6$ and $SiH_3 + Si_2H_5$ reactions and the thermal unimolecular decomposition of Si_3H_8 for all low-energy paths have been calculated with multichannel variational RRKM theory covering varying *P*,*T* conditions typically employed in PECVD and Cat-CVD processes for hydrogenated amorphous silicon (a-Si/H) film growth. The results were also found to be in good agreement with available kinetic data. Our kinetic results may be employed to model and control very large-area a-Si/H film growth for a new generation of solar cell applications.

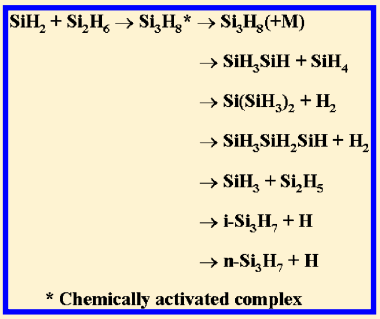

INTRODUCTION

Silylene, SiH_2, plays an important role in the reactions of silane or disilane forming higher silanes in the deposition of hydrogenated amorphous silicon (a-Si/H) thin films and polycrystalline silicon (p-Si).[1−6] For many decades, the technology has been used in the semiconductor industry for fabrication of solar cells, thin film transistors, and so on.[7,8] These films are prepared either by plasma-enhanced chemical vapor deposition (PECVD) or, increasingly, by catalytic chemical vapor deposition (Cat-CVD).[1−12] In both processes, silanes and hydrogen are employed as the source gases in a chamber. From the mechanistic point of view, the dissociation of a silane source gas, by collisions with electrons in a plasma or with a hot metal catalyst surface, leads to the generation of radicals, atoms, and ions. These species diffuse on to the substrate after the secondary reactions in the gas phase, depositing a-Si/H film through surface reactions. The chemical processes of the amorphous material formation thus involve gas-phase and surface reactions, which are affected by the system's temperature and have a strong influence on the quality of the film. Roth et al. investigated the gas-phase parameters such as the flow, temperature, and pressure of participating reactants; the energy input for dissociation reactions, the size, and the structure of Si−H compounds have an important influence on the properties of the surface layer.[13]

Mechanistically, SiH_2 is known to be a primary decomposition product in the decomposition of silanes.[1−19] The interaction of the SiH_2 radical with Si_2H_6 is a subject of interest in the present work because Si_2H_6 is one of the most commonly employed reagents and silylene is known to be a very reactive diradical that inserts into Si−H bonds very efficiently, forming excited adduct Si_3H_8.[14−19] The excited adduct can dissociate via intramolecular 1,2-H shifts, producing various products.[20−22] Inoue et al.[16] detected SiH_2 by laser-induced fluorescence and found the rate constants of the SiH_2 reaction with Si_2H_6 to be 5.7×10^{-10} cm^3 $molecule^{-1}$ s^{-1} in 1 Torr of helium at room temperature. Later, Jasinski et al.[17] generated SiH_2 by using laser absorption spectroscopy and found the overall rate constant of the SiH_2 with disilane reaction from 1 to 10 Torr of He pressure at 298 K; the rate constant measured at 1 Torr of pressure was 1.5×10^{-10} cm^3 $molecule^{-1}$ s^{-1}. Ditrich et al.[4] investigated the role of silylene in the laser-induced CVD of a-Si/H and the rate constant of SiH_2 with silane or disilane, forming higher silanes, Si_2H_6 and Si_3H_8. The rate constant for formation of the latter product was measured under the deposition condition to be $2.7 \pm 0.4 \times 10^{-10}$ cm^3 $molecule^{-1}$ s^{-1}.

Received: July 29, 2013
Revised: September 14, 2013
Published: September 23, 2013

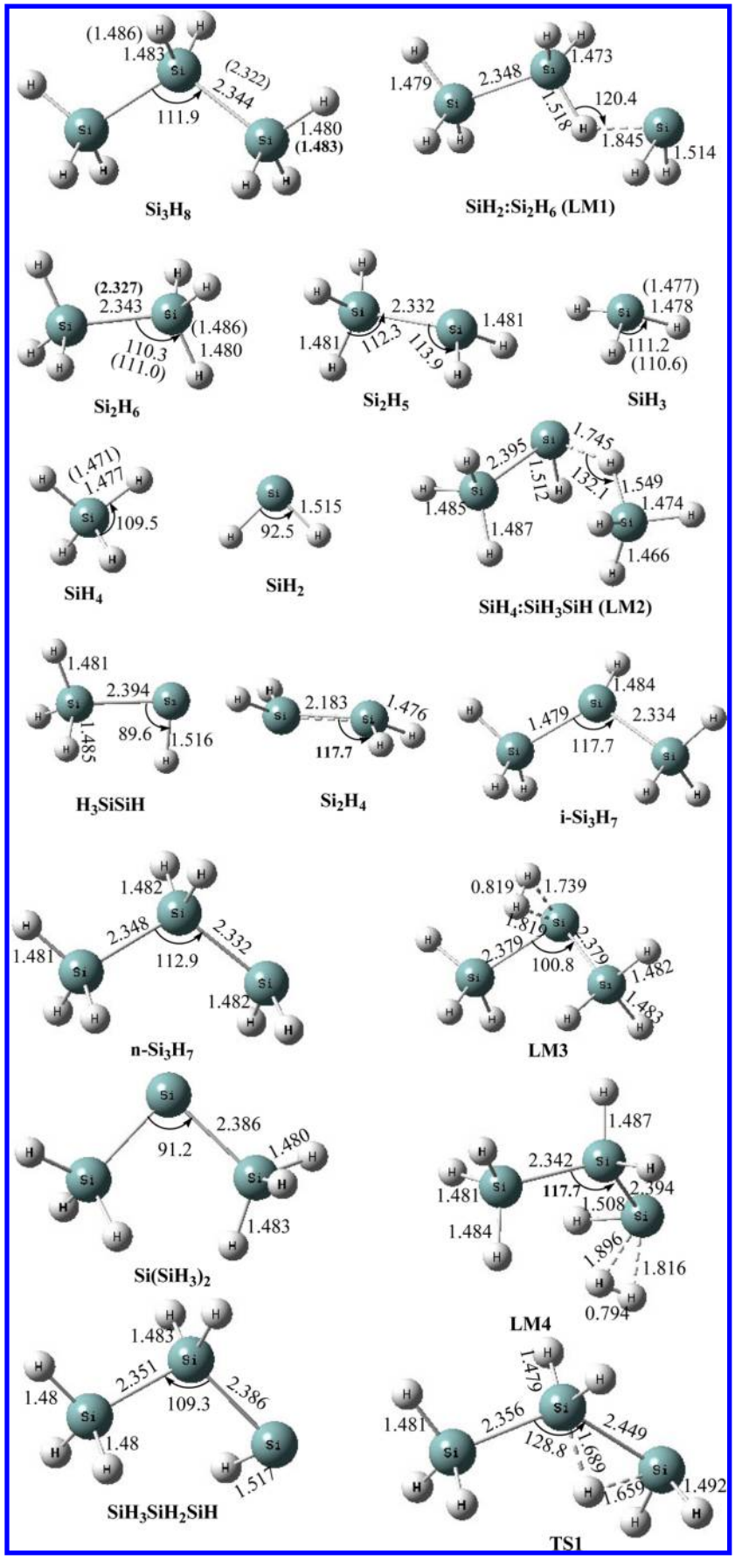

Figure 1. continued

dx.doi.org/10.1021/jp407553a | J. Phys. Chem. A 2013, 117, 10811−10823

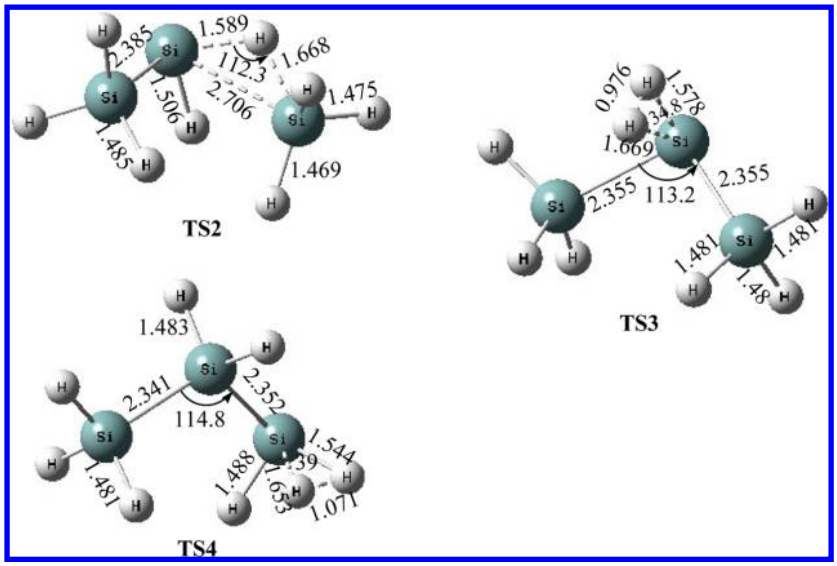

Figure 1. The optimized geometries of the reactants, intermediates, transition states, and products computed at the QCISD/6-311++G(d,p) level. The values in parentheses are the experimental values (refs 39 and 40). (Lengths in Å, and angles in degrees.)

Absolute rate constants for the reactions of SiH_2 with Si_2H_6 have also been determined by Walsh and co-workers,[18] covering the temperature range of 295−595 K by means of laser flash photolysis. Ring, O'Neal, and co-workers interpreted the mechanism for decomposition of Si_3H_8 in the temperature range of 529−560 K.[20,21] Arrhenius parameters for Si_3H_8 decomposition via 1,2-hydrogen migration reactions that lead to disilane and silylene at 530−570 K have been measured by Moffat et al.[22]

Various works have been carried out with Si_2H_6 and Si_3H_8 as source gases for the preparation of a-Si/H thin films by low-temperature CVD.[23,24] Kumata et al.[23] investigated the deposition rate of a-Si/H films prepared from Si_3H_8 by the direct photo-CVD method, which was found to be five times that from Si_2H_6. In our earlier studies, we used computational tools to elucidate reaction mechanisms and provide accurate thermodynamic and kinetics data for gas-phase reactions of SiH_3, SiH_4, Si_2H_6, and Si_3H_8 with H and SiH_3.[25−28] These species are known to coexist in media under CVD conditions.

Under experimental conditions, the generated radicals and ions in the reaction chamber undergo a variety of primary and secondary reactions leading to reaction products, which are potential candidates for the layer-forming process at the substrate surface. It is well-known that SiH_2 is easily generated in the electron-impact dissociation reaction of silane and hydrogen. Therefore, a detailed understanding of the gas-phase reactions involved may be useful to control the deposition parameters for optimization of the a-Si/H growth in a large substrate area under well-defined conditions. In this work, we focus our study on the effects of temperature and pressure on the association reactions of $SiH_2 + Si_2H_6$ and $SiH_3 + Si_2H_5$ via the Si_3H_8 intermediate for both forward and reverse processes, which are critical to our ability in realistic simulations of a-Si−H thin film growth by PECVD and Cat-CVD. We will study the detailed mechanism for the title reactions by fully characterizing their common potential energy surface (PES), employing ab initio molecular orbital methods. For the SiH_2 and Si_2H_6 reaction, it may take place by the following channels in the forward and reverse directions:

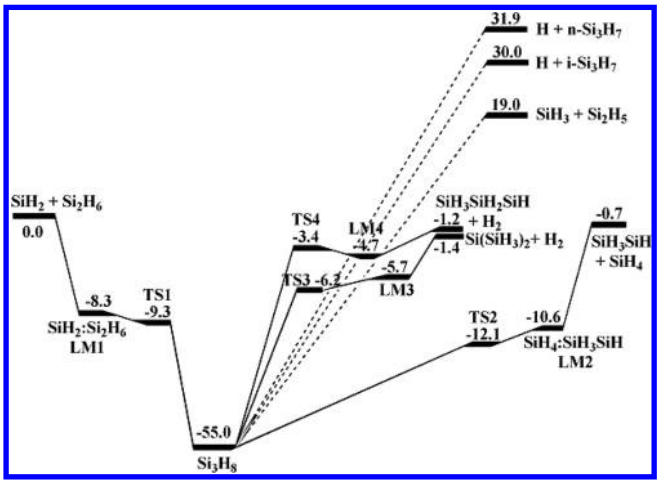

Figure 2. Schematic energy diagram for the $SiH_2 + Si_2H_6$ reaction computed at the QCISD(T)/CBS//QCISD/6-311++G(d,p) level with ZPE corrections. Relative energies are given in kcal/mol at 0 K.

$$SiH_2 + Si_2H_6 \rightarrow Si_3H_8^* \rightarrow Si_3H_8(+M) \quad (1)$$

$$\rightarrow SiH_4 + SiH_3SiH \quad (2)$$

$$\rightarrow H_2 + Si(SiH_3)_2 \quad (3)$$

$$\rightarrow H_2 + SiH_3SiH_2SiH \quad (4)$$

$$\rightarrow SiH_3 + Si_2H_5 \quad (5)$$

On the same PES, SiH_3 and Si_2H_5 radicals produced from the fragmentation of Si_3H_8* depicted above may react as follows in a deposition medium:

$$SiH_3 + Si_2H_5 \rightarrow Si_3H_8^* \rightarrow Si_3H_8(+M) \quad (6)$$

$$\rightarrow SiH_2 + Si_2H_6 \quad (7)$$

$$\rightarrow SiH_4 + SiH_3SiH \quad (8)$$

$$\rightarrow H_2 + Si(SiH_3)_2 \quad (9)$$

$$\rightarrow H_2 + SiH_3SiH_2SiH \quad (10)$$

In the above reaction schemes, * denotes an internally activated intermediate and M stands for a third body or

dx.doi.org/10.1021/jp407553a | J. Phys. Chem. A 2013, 117, 10811−10823

Table 1. Calculated Relative Energies (kcal/mol, ZPE corrections are included) for the SiH_2 Reaction with Si_2H_6 at Various Levels of Theory

	QCISD/6-311++G(d,p)	QCISD(T)/6-311++G(3df,2p)[a]	QCISD(T)/CBS[a]
$SiH_2 + Si_2H_6$	0.0	0.0	0.0
SiH_2/Si_2H_6, LM1	−4.3	−7.0	−8.3
TS1	−1.5	−6.8	−9.3
Si_3H_8	−50.0	−52.7	−55.0
TS2	−4.8	−10.1	−12.2
SiH_4/SiH_3SiH, LM2	−4.8	−9.0	−10.6
$SiH_4 + SiH_3SiH$	0.2	−0.6	−0.7
TS3	3.4	−3.8	−6.2
$H_2/Si(SiH_3)_2$, LM3	3.8	−3.9	−5.7
$H_2 + Si(SiH_3)_2$	3.8	−1.7	−1.4
TS4	5.7	−0.9	−3.4
H_2/SiH_3SiH_2SiH, LM4	3.0	−3.3	−4.7
$H_2 + SiH_3SiH_2SiH$	2.5	−1.7	−1.2
$SiH_3 + Si_2H_5$	17.7	19.0	19.0
H + *i*-Si_3H_7	31.7	29.9	30.0
H + *n*-Si_3H_7	33.6	31.8	31.9

[a]Single-point calculations based on QCISD/6-311++G(d,p) optimized geometries.

quencher. The predicted geometries, vibrational frequencies, and heats of formation for new radical products at 0 K are given in the Results and Discussion section. The temperature and pressure dependences of the rate constants for the forward and reverse reactions and their related unimolecular decomposition processes have been derived using variational RRKM theory by solving the master equation covering the conditions commonly employed in industrial deposition of a-Si/H films.

COMPUTATIONAL METHODS

The geometries of the reactants, products, intermediates, and transition states of the title reactions have been fully optimized by using the QCISD method[29] (the spin-unrestricted quadratic configuration interaction with single and double excitation) with the 6-311++G(d,p) basis set. Further improvement of energetics of the PES has been made with QCISD(T)/6-311++G(3df,2p) by single-point calculations. Vibrational frequencies calculated at the QCISD/6-311++G(d,p) level have been used for characterization of stationary points, zero-point energy (ZPE) corrections, and reaction rate constants calculations. A recent study on silicon species has shown that the widely used QCISD method with split valence and Dunning correlation basis sets is quite suitable for geometry and property predictions.[30,31] For a more accurate evaluation of the energetic parameters, single-point energy calculations of the stationary points were carried out by the QCISD(T)/CBS method,[32] in which the basis set extrapolation was based on the calculations with the cc-pVXZ (X = D, T, and Q) basis sets of Dunning.[33] The CBS energies were estimated by the three-point extrapolation scheme.[32] All of the calculations were carried out using the Gaussian 03 program package.[34]

Rate constant calculations were carried out with the VARIFLEX program[35] based on the microcanonical RRKM theory and variational transition-state theory (VTST).[36,37] The component rates were evaluated at the E/J-resolved level, and the pressure dependence was treated by one-dimensional master equation calculations using the Boltzmann probability of the intermediate (Si_3H_8*) for the J-distribution. For a barrierless association/decomposition process, the variational TS[36,37] was approximated with the Morse function, $V(R) = D_e\{1 - \exp[-\beta(R - R_e)]\}^2$, in conjunction with a potential anisotropy function to represent the minimum potential energy path (MEP), which will be discussed later. Here, D_e is the binding energy excluding zero-point vibrational energy for an association reaction, R is the reaction coordinate (i.e., the distance between the two bonding atoms), and R_e is the equilibrium value of R at the stable intermediate structure.

Table 3. Predicted Morse (β) and Exponential Coefficient Lennard-Jones Parameters Used in Rate Constant Calculations

		Lennard-Jones parameters[47]		
reactions	Morse (β) (Å)		σ (Å)	ε (cm^{-1})
$Si_3H_8 \rightarrow SiH_3 + Si_2H_5$	1.68	Si_3H_8	5.563	230.05
LM1 → $SiH_2 + Si_2H_6$	1.73	Ar	3.75	98.3
LM2 → $SiH_4 + SiH_3SiH$	1.66	He	2.55	10.22
LM3 → $H_2 + Si(SiH_3)_2$	1.86			
LM4 → $H_2 + SiH_3SiH_2SiH$	1.89			

Table 2. Heats of Reaction ($\Delta_r H_0°$) and Heats of Formation ($\Delta_f H_0°$) of Species at 0 K Predicted at The QCISD/6-311++G(d,p)/CBS Level of Theory Given in kcal/mol

		heat of reaction $\Delta_r H_0°$		heat of formation $\Delta_f H_0°$	
species	reactions[a]	calculated	literature[a]	calculated	literature[a]
Si_3H_8	$^1SiH_2 + Si_2H_6 \rightarrow Si_3H_8$	−55.0	−55.0	33.5	33.5 ± 1.0
SiH_3	$Si_3H_8 \rightarrow SiH_3 + Si_2H_5$	74.0	73.4	48.3	47.7 ± 1.2
SiH_3SiH	$Si_3H_8 \rightarrow SiH_4 + SiH_3SiH$	54.3		77.3	
Si_2H_4	$Si_3H_8 \rightarrow SiH_4 + Si_2H_4$	45.0	47.0 ± 1.0	68.0	67.9 ± 0.9
i-Si_3H_7	$Si_3H_8 \rightarrow H + i\text{-}Si_3H_7$	85.1	86	66.9 ± 1.0	67.8
n-Si_3H_7	$Si_3H_8 \rightarrow H + n\text{-}Si_3H_7$	86.9	87.5	68.7 ± 1.0	69.3
$Si(SiH_3)_2$	$Si_3H_8 \rightarrow H_2 + Si(SiH_3)_2$	53.6		87.1	
SiH_3SiH_2SiH	$Si_3H_8 \rightarrow H_2 + SiH_3SiH_2SiH$	53.8		87.3	

[a]The experimental values employed in the calculations are obtained based on the enthalpies of formation at 0 K for H = 51.7 kcal/mol; H_2 = 0.0 kcal/mol; SiH_4 = 10.5 kcal/mol (ref 42); SiH_3 = 47.7 ± 1.2 kcal/mol (ref 42); $^1SiH_2$ = 65.6 ± 0.7 kcal/mol (ref 42); Si_3H_8 = 33.5 ± 1.0 kcal/mol (ref 26); Si_2H_6 = 22.9 kcal/mol (refs 41−43); Si_2H_5 = 59.2 kcal/mol (ref 43); *i*-Si_3H_7 = 67.8 kcal/mol (refs 41 and 26); *n*-Si_3H_7= 69.3 kcal/mol (refs 41 and 26); and Si_2H_4 = 67.9 ± 0.9 (ref 43).

dx.doi.org/10.1021/jp407553a | J. Phys. Chem. A 2013, 117, 10811−10823

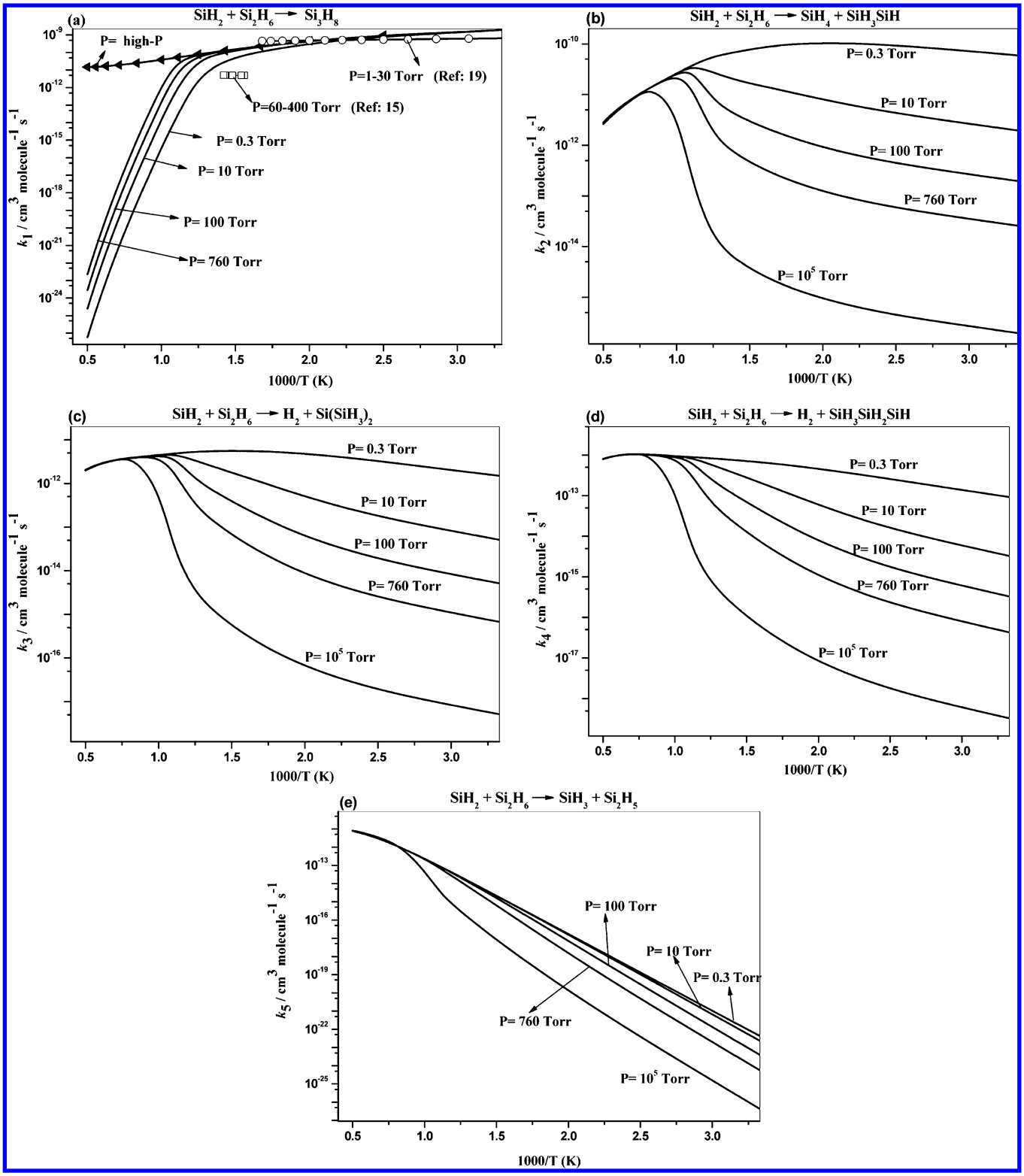

Figure 3. Arrhenius plots of rate constants for the $SiH_2 + Si_2H_6$ reaction forming various products, Si_3H_8 (a), $SiH_4 + SiH_3SiH$ (b), $H_2 + Si(SiH_3)_2$ (c), $H_2 + SiH_3SiH_2SiH$ (d), and $SiH_3 + Si_2H_5$ (e), at different pressures.

The Morse function was characterized variationally from the optimized bond length to separated radical pairs with an interval of 0.1 Å by second-order multireference perturbation theory (CASPT2//CASSCF(8,8)/6-311+G(3df,2p) level). Other geometric parameters were fully optimized. These calculations were performed with the MOLPRO code.[38]

RESULTS AND DISCUSSIONS

PES and Reaction Mechanism. The optimized geometries of reactants, intermediates, transition states, and products are shown in Figure 1, along with the available experimental bond lengths.[39] As aforementioned, the PES of the Si_3H_8 system was predicted at the QCISD(T)/CBS//QCISD/6-311++G(d,p) + ZPVE level

dx.doi.org/10.1021/jp407553a | J. Phys. Chem. A 2013, 117, 10811−10823

Table 4. Arrhenius Parameters[a] for the Bimolecular Reaction of SiH_2 with Si_2H_6 Giving Different Products at Various Pressures and Temperature Including High-Pressure (k_∞) and Low-Pressure (k_0) Limits

products	P (Torr)	A	n	E_a/R (K)	k_p(500 K)
Si_3H_8 (k_1)	k_∞	2.55×10^{7}	−5.83	1141	4.64×10^{-10}
	k_0	5.51×10^{1}	−9.2	2565	5.76×10^{-26}
	0.3	1.60×10^{20}	−10.2	2565	3.34×10^{-10}
	1	1.36×10^{15}	−8.4	2023	4.01×10^{-10}
	10	2.82×10^{9}	−6.5	1381	4.54×10^{-10}
	760	3.54×10^{7}	−5.9	1158	4.64×10^{-10}
$SiH_4 + SiH_3SiH$ (k_2)	k_0	9.11×10^{-15}	−3.6	2209	1.86×10^{-26}
	1	2.97×10^{-04}	−2.0	1509	5.14×10^{-11}
	10	1.28×10^{-20}	3.2	−180	7.92×10^{-12}
	760	5.95×10^{-33}	6.7	−1409	1.18×10^{-13}
$H_2 + Si(SiH_3)_2$ (k_3)	k_0	5.56×10^{-22}	−1.6	1866	8.53×10^{-28}
	1	1.85×10^{-11}	0.1	1225	2.67×10^{-12}
	10	3.98×10^{-30}	6.1	−649	4.97×10^{-13}
	760	1.55×10^{-47}	11.3	−2460	8.09×10^{-15}
$H_2 + SiH_3SiH_2SiH$ (k_4)	k_0	9.00×10^{-27}	−0.22	1678	8.09×10^{-29}
	1	4.36×10^{-15}	1.05	1222	2.76×10^{-13}
	10	1.15×10^{-34}	7.4	−705	5.84×10^{-14}
	760	1.38×10^{-54}	13.5	−2789	1.02×10^{-15}
$SiH_3 + Si_2H_5$ (k_5)	k_0	4.17×10^{-28}	1.18	9616	2.92×10^{-33}
	1	2.39×10^{-9}	0.09	9667	1.69×10^{-17}
	10	3.15×10^{-5}	−1.17	10529	1.56×10^{-17}
	760	1.68×10^{-27}	6.13	8769	1.48×10^{-18}

[a] $k(T) = AT^n \exp(-E_a/RT)$ predicted for various temperatures 300−600 K in units of cm^3 $molecule^{-1}$ s^{-1} for k and k_∞ and cm^6 $molecule^{-2}$ s^{-1} for k_0.

Table 5. Arrhenius Parameters[a] for the Bimolecular Reaction of SiH_3 with Si_2H_5 Giving Different Products at Various Pressures and Temperatures Including High-Pressure (k_∞) and Low-Pressure (k_0) Limits

products	P (Torr)	temp (K)	A	n	E_a/R (K)	k_p(500 K)
Si_3H_8 (k_6)	k_∞	300−600	3.94×10^{-10}	0.11	51	6.93×10^{-10}
	k_0	300−600	6.36×10^{10}	−14.3	2634	6.78×10^{-31}
	0.3	300−600	1.84×10^{29}	−15.3	2634	3.93×10^{-15}
	1	300−600	4.45×10^{32}	−15.7	3237	2.24×10^{-13}
	10	300−600	8.11×10^{26}	−12.7	3543	4.89×10^{-11}
$SiH_2 + Si_2H_6$ (k_7)	k_0	300−600	7.23×10^{-29}	0.97	132	2.31×10^{-26}
	1	300−600	2.68×10^{-10}	−0.06	156	1.34×10^{-10}
	10	300−600	1.71×10^{-6}	−1.22	977	1.23×10^{-10}
	760	300−600	1.53×10^{-28}	6.01	−755	1.18×10^{-11}
$SiH_4 + SiH_3SiH_2$ (k_8)	k_0	300−600	3.48×10^{-27}	0.55	200	7.13×10^{-26}
	1	300−500	7.48×10^{-9}	−0.4	190	4.14×10^{-10}
	10	300−600	3.08×10^{-4}	−1.83	1102	3.90×10^{-10}
	760	300−600	2.48×10^{-26}	5.41	−644	3.69×10^{-11}
$H_2 + Si(SiH_3)_2$ (k_9)	k_0	300−600	3.03×10^{-31}	1.77	−50.7	2.0×10^{-26}
	1	300−600	2.35×10^{-12}	0.64	27.2	1.16×10^{-10}
	10	300−600	1.18×10^{-8}	−0.49	847	1.04×10^{-10}
	760	300−600	7.62×10^{-31}	6.8	−888	1.02×10^{-11}
$H_2 + SiH_3SiH_2SiH$ (k_{10})	k_0	300−600	1.08×10^{-33}	2.41	−178.8	4.83×10^{-27}
	1	300−600	1.03×10^{-14}	1.24	−81.6	2.78×10^{-11}
	10	300−600	5.47×10^{-11}	0.11	753	2.48×10^{-11}
	760	300−600	2.68×10^{-33}	7.45	−981.7	2.47×10^{-12}

[a] $k(T) = AT^n \exp(-E_a/RT)$ predicted for various temperatures in units of cm^3 $molecule^{-1}$ s^{-1} for k and k_∞ and cm^6 $molecule^{-2}$ s^{-1} for k_0.

of theory, as shown in Figure 2. The corresponding energies estimated at different levels of the theory are summarized in Table 1. The moments of inertia and the vibrational frequencies of all of the species involved in these reactions are listed in the Supporting Information Table S1 for the kinetic calculations. The calculated heats of reaction and formation values are given in Table 2 and are compared with available experimental data at 0 K. Discussion of the thermochemical data will be made later. The following discussion on the PES will be based on the energies of the TSs and intermediates relative to the reactants computed at the QCISD(T)/CBS//QCISD level.

SiH_2 + Si_2H_6 Reaction. As shown in Figure 2, the initial association reaction of SiH_2 and Si_2H_6, proceeding via the van der Waals complex, SiH_2/Si_2H_6 (LM1) with an 8.3 kcal/mol binding energy, can readily occur by an insertion reaction into one of the Si−H bonds in Si_2H_6 from the side with a somewhat

dx.doi.org/10.1021/jp407553a | J. Phys. Chem. A 2013, 117, 10811−10823

smaller activation barrier via TS1 forming Si_3H_8; the process is exothermic by 55.0 kcal/mol at the QCISD(T)/CBS//QCISD level. It should be noted that previous studies also reported a similar smaller activation energy.[2,3] The ground electronic state of SiH_2 is singlet, not triplet as in the CH_2 case. We considered Si_3H_8 and TS1 as a singlet state. The TS1 calculated at QCISD/6-311++G(d,p) and QCISD(T)/6-311++G(3df,2p)//QCISD/6-311++G(d,p) levels have small positive barriers of 2.8 and 0.2 kcal/mol, respectively, when compared to LM1 (see Table 1). The predicted Gibbs free energy of activation at 298 K from LM1 to TS1 was found to be positive also. Walsh's group theoretically explored the mechanism of the Si−H insertion process by silylene. They explained that silylene has an empty p orbital and a lone pair of electrons. The electron density is transferred from the Si−H bond of silane to the empty p orbital of silylene, and simultaneously, the lone pair of electrons in silylene is donated to the Si of silane to produce the new Si−Si bond. As aforementioned, the two processes occur with the involvement of an intermediate complex.[18,19] As shown in Figure 1, LM1 has C_1 symmetry, and SiH_2 is located with Si pointing toward a Si−H bond in the Si_2H_6 molecule at a distance of 1.845 Å. However, TS1 lies 9.3 kcal/mol below the reactants, and their structure has a tighter three-membered ring, in which the forming H−Si and Si−Si bond lengths are 1.659 and 2.449 Å, respectively, and the Si−H breaking bond length is elongated to 1.689 Å, which is 0.209 Å longer than that of Si_2H_6.

SiH_3 + Si_2H_5 Reaction. Both SiH_3 and Si_2H_5 radicals formed in the SiH_2 + Si_2H_6 reaction may coexit in the plasma-induced reactions of small silanes (SiH_4, Si_2H_6, and Si_3H_8, for example). The PES shown in Figure 2 suggests that all product pairs that lie below SiH_3 + Si_2H_5 can be accessed and produced in the reaction, as listed in the Introduction (i.e., reactions 6−10).

Decomposition of Si_3H_8. The initially formed chemically activated Si_3H_8 adduct may eliminate several products, SiH_4, SiH_3, H_2, and H, directly, as shown in Figure 2. In the Si_3H_8 decomposition reactions, the lowest-energy channel producing SiH_4 + H_3SiSiH lies 54.3 kcal/mol above Si_3H_8. The 2,1-H shift occurs by migration of one of the H atoms in the secondary SiH_2 group to the SiH_3 group to form a van der Waals complex, SiH_4/SiH_3SiH, LM2, via TS2. The barrier height at TS2 is 42.8 kcal/mol, and the complex is 44.4 kcal/mol above Si_3H_8. The energies of TS2 predicted at the QCISD/6-311++G(d,p) and QCISD(T)/6-311++G(3df,2p)//QCISD/6-311++G(d,p) levels are 45.2 and 42.6 kcal/mol, respectively. The latter is close to the CBS limit, 42.8 kcal/mol. We also calculated the SiH_4/SiH_3SiH, LM2 energy with other methods; when compared with TS2 at the QCISD/6-311++G(d,p) level, LM2 has the same energy while at the QCISD(T)/6-311++G(3df,2p)//QCISD/6-311++G(d,p) level, it is 1.1 kcal/mol above TS2. Here, although the transition state has a lower activation barrier compared with the complex, our result is consistent with previous reports.[2,3] The predicted Gibbs free energy of activation at 298 K from LM2 to TS2 was found to be positive also. At TS2, the bond lengths of the breaking Si···H and Si···Si were predicted to be 1.589 and 2.706 Å, respectively, and the forming H···SiH_3 bond was predicted to be 1.668 Å calculated by the QCISD/6-311++G(d,p) method (Figure 1). In addition, the Si_2H_4 + SiH_4 products may be formed by H_3SiSiH isomerization with a small 1.6 kcal/mol barrier. Our result presented in Figure 2 shows that in the Si_3H_8 dissociation reaction, the secondary H-atom shifting to form SiH_4 has a lower activation energy when compared to that of the primary H-atom shifting

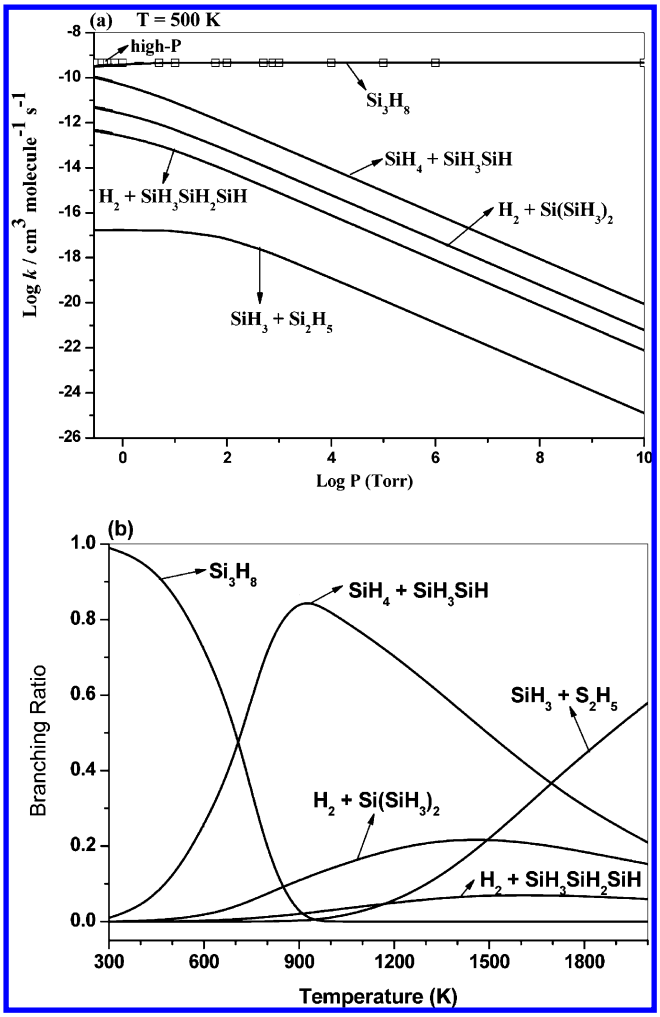

Figure 4. (a) Pressure dependences of all product channels of SiH_2 + Si_2H_6 reaction rate constants at T = 500 K as functions of pressure. (b) Branching ratios of SiH_2 + Si_2H_6 reaction products at 1 Torr of pressure.

to form SiH_2. This mechanism is in good agreement with previous experimental work.[1] Si_2H_4 is a stable and potential candidate for film formation.[4] As shown in Figure 2, the interaction of the two H atoms at the secondary Si position in Si_3H_8 can eliminate H_2 via a three-membered-ring transition state TS3 (48.8 kcal/mol) to form a van der Waals complex, $Si(SiH_3)_2/H_2$, LM3. At TS3, the two breaking Si−H bonds lengthen unequally from 1.483 Å in Si_3H_8 to 1.578 and 1.669 Å; the forming H−H bond length is 0.976 Å. Relative to SiH_2 + Si_2H_6, the reaction product $Si(SiH_3)_2$ + H_2 is exothermic by 1.4 kcal/mol. Similarly, as shown in Figure 2, H_2 elimination can also take place at a terminal Si atom of Si_3H_8 to form a SiH_3SiH_2SiH + H_2 via TS4 and the SiH_3SiH_2SiH/H_2, LM4 complex. The barrier height at TS4 is 51.6 kcal/mol, and the complex is 50.3 kcal/mol above Si_3H_8. The H_2 elimination barrier from the secondary Si atom in Si_3H_8 is thus 2.8 kcal/mol lower compared with that from a terminal SiH_3 group.

On this PES, the next lowest-energy product channel is SiH_3 + Si_2H_5, formed by direct cleaving of one of the Si−Si bonds in Si_3H_8, requiring as much as 74.0 kcal/mol. The predicted heat of reaction is in good agreement with available experimental and computed values,[25−28,39,40] as shown in Table 2. This process does not have a well-defined transition state. Due to the

dx.doi.org/10.1021/jp407553a | J. Phys. Chem. A 2013, 117, 10811−10823

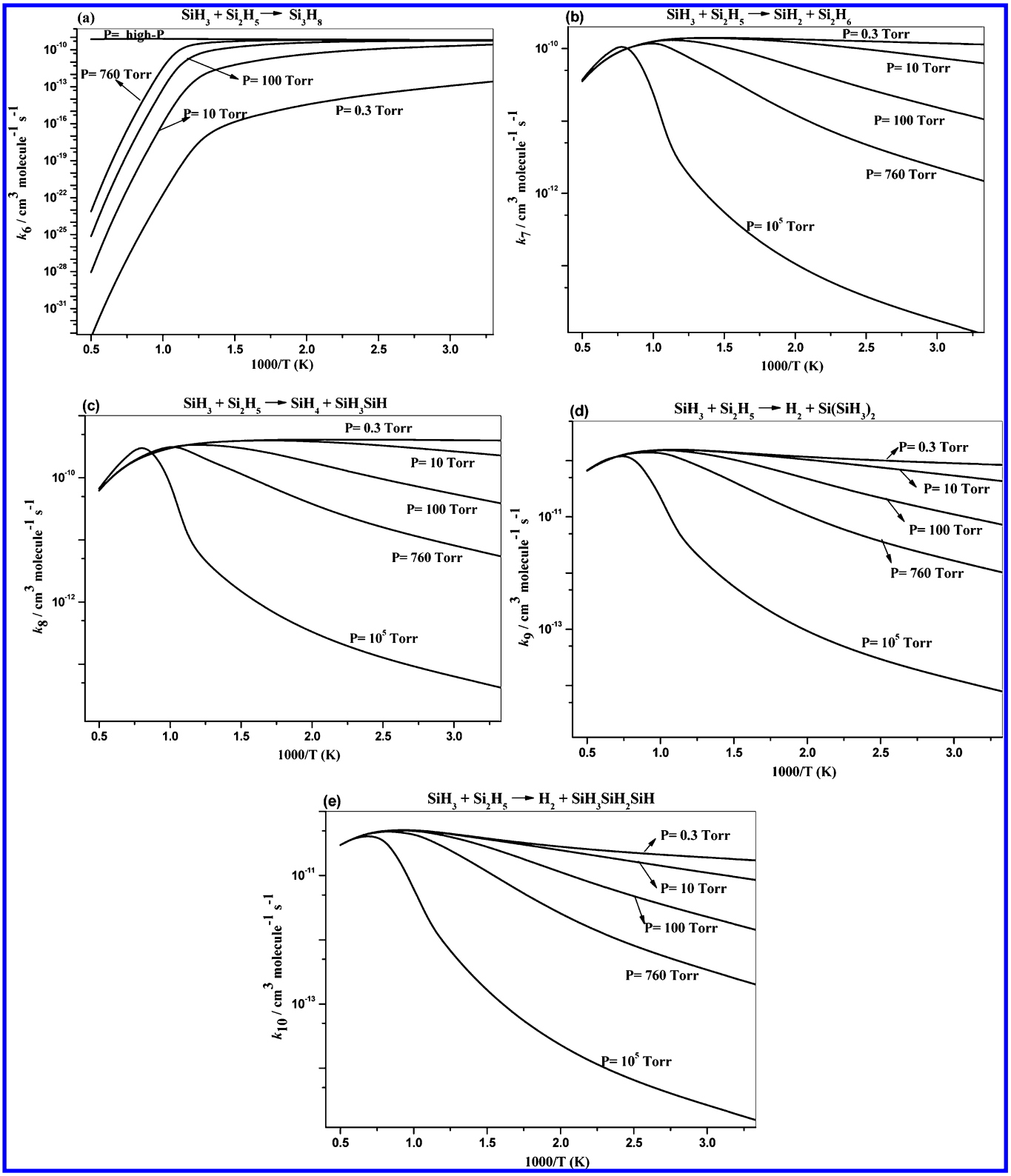

Figure 5. Arrhenius plots of rate constants for the $SiH_3 + Si_2H_5$ reaction forming various products Si_3H_8 (a), $SiH_2 + Si_2H_6$ (b), $SiH_4 + SiH_3SiH$ (c), $H_2 + Si(SiH_3)_2$ (d), and $H_2 + SiH_3SiH_2SiH$ (e) at different pressures.

absence of an intrinsic transition state for the fragmentation reaction, its dissociation potential function was computed variationally to cover a range of Si−Si separations from the equilibrium value 2.344 to 6.5 Å with an interval of 0.1 Å by second-order multireference perturbation theory (CASPT2) based on the CASSCF optimized geometries with eight active electrons and eight active orbitals using the 6-311+G(3df,2p) basis set. Aforementioned in the above section, other geometric parameters were fully optimized. These calculations were performed with the MOLPRO code.[38] The computed potential

dx.doi.org/10.1021/jp407553a | J. Phys. Chem. A 2013, 117, 10811−10823

energies could be fitted to the Morse function with the parameters of β = 1.68 Å^{-1} (SiH_3 + Si_2H_5), for Si−Si bond breaking. In the same manner, with much computational effort, we also determined the values β = 1.73, 1.66, 1.86, and 1.89 Å^{-1} from LM1 to SiH_2 + Si_2H_6, LM2 to SiH_4 + SiH_3SiH, LM3 to H_2 + $Si(SiH_3)_2$, and LM4 to H_2 + SiH_3SiH_2SiH, respectively. These values will be used in the rate constant calculations to be discussed below. In the formulation of the Morse potential, r is the distance between the two bonding atoms for the separation of two fragments. As shown in the PES of Figure 2, H_2 is produced via LM3 and LM4. The reactions involved are reactions 3, 4, 9, and 10, shown in the reaction scheme. In these calculations, the separation "r" begins with the smaller of the two Si···H bonds from its equilibrium separation to about 4.5 Å at an interval of 0.1 Å. As the VTSs are typically located at 2.5−3.5 Å, the values of r based on this method or the H_2 center-of-mass separation from the Si involved are essentially the same; so are the values of the rate constant predicted. Finally, the cleavage of the secondary and primary Si−H bonds in the Si_3H_8 giving rise to the products H + i-Si_3H_7 and H + n-Si_3H_7 are predicted to be endothermic by 82.6 and 84.5 kcal/mol, respectively, without intrinsic barriers (see Figure 2).

Enthalpies of Formation. The predicted heats of formation of all of the species related to the SiH_2 reaction with Si_2H_6 and the unimolecular decomposition of Si_3H_8 are presented in Table 1 based on the energies computed at the QCISD/6-311++G(d,p), QCISD(T)/6-311++G(3df,2p)//QCISD/6-311++G(d,p) and QCISD(T)/CBS//QCISD/6-311++G(d,p) levels. As one would expect, the last two higher-level methods give rise to values closer to each other. The heats of formation were determined by combining the computed heats of reaction ($\Delta_r H_0°$) based on the CBS limit values and experimental heats of formation ($\Delta_f H_0°$) of other species involved in the reaction at 0 K. Theoretically, the heats of formation of Si_3H_8, n-Si_3H_7, and i-Si_3H_7 are available in the literature as 33.5 ± 1.0, 38.3, and 37.5 kcal/mol, respectively, at 0 K, as referenced in the footnote of Table 2. Thus, by using these values and experimental heats of formation, we obtained the values at 0 K for SiH_3SiH, Si_2H_4, $Si(SiH_3)_2$, and SiH_3SiH_2SiH to be 77.3, 68.0, 87.1, and 87.3 kcal/mol, respectively, with an estimated error of ±1.2 kcal/mol. Our predicted heats of formation of the species listed in Table 2 are in good agreement with the values derived from available experimental and theoretical data.[25−28,41−43]

Rate Constant Calculations. The rate constants for the bimolecular reactions SiH_2 + Si_2H_6 and SiH_3 + Si_2H_5 and the related unimolecular decomposition processes can be computed with the predicted PES using energies obtained by QCISD(T)/CBS extrapolation and the QCISD/6-311++G(d,p) molecular parameters of the reactants, intermediates, and transition states presented in Table S1 in the Supporting Information. The rate constants for the forward reactions of SiH_2 + Si_2H_6 via the low-energy channels have been computed in the temperature range of 300−2000 K and the pressure range of 0.3−760 Torr with the Variflex code, whereas the higher-energy H-production channels are neglected. The VTST calculations were carried out with the unified statistical formulation of Miller[44] including multiple reflection corrections[45,46] above the shallow wells of the prereaction and postreaction complexes LM1, LM2, LM3, and LM4. The Lennard-Jones parameters for collision rate estimates are obtained by using σ and ε and are given in Table 3.[47] The P,T conditions studied cover most of the conditions employed in PECVD (typically 0.75−4 Torr, 373−723 K) and Cat-CVD (typically 0.1−10 Torr, 473−673 K)[9−12]

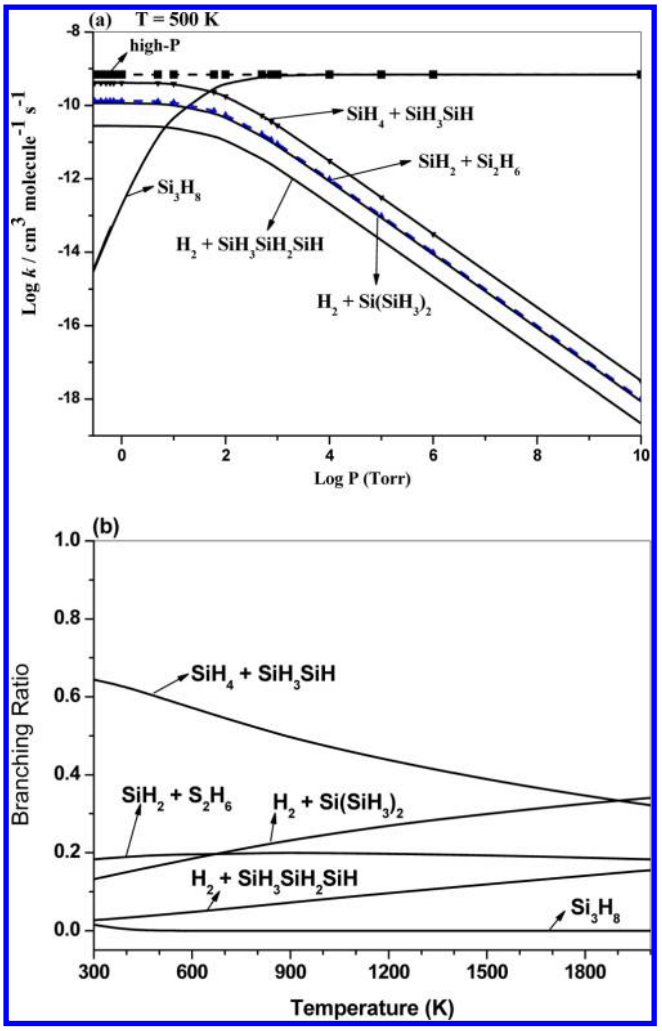

Figure 6. (a) Pressure dependences of all product channels of SiH_3 + Si_2H_5 reaction rate constants at T = 500 K as functions of pressure. (b) Branching ratios of SiH_3 + Si_2H_5 reaction products at 1 Torr of pressure.

Rate Constant for SiH_2 + Si_2H_6. The bimolecular reaction of SiH_2 and Si_2H_6 occurs exclusively by the insertion process forming the excited Si_3H_8 intermediate carrying as much as 55.0 kcal/mol of internal energy with 12.1 kcal/mol of excess energy above the transition state for 1,2-H elimination at TS2, giving the SiH_4 and SiH_3SiH radical, as shown by the PES given in Figure 2. The predicted rate constants for all of the product channels represented by reactions 1−5 listed in the Introduction at various pressures between 0.3 and 760 Torr along with the high pressure limit in the temperature range of 300−2000 K are graphically presented in Figure 3 and are also listed in Table 4, covering the temperature range 300−600 K. In the rate constant calculation, the internal rotation of the SiH_3 group of Si_3H_8 with the vibrational frequency of 77 cm^{-1} is hindered by a 1.0 kcal/mol barrier and thus also treated as a hindered rotor.

As shown in Figure 3a, under the high-pressure condition, the reaction occurs primary by a recombination/stabilization process producing Si_3H_8. Our predicted absolute rate constants for Ar buffer gas agree quite well with experimental data.[15−19] Walsh and co-workers[18,19] reported the values of 3.04 × 10^{-10}

dx.doi.org/10.1021/jp407553a | J. Phys. Chem. A 2013, 117, 10811−10823

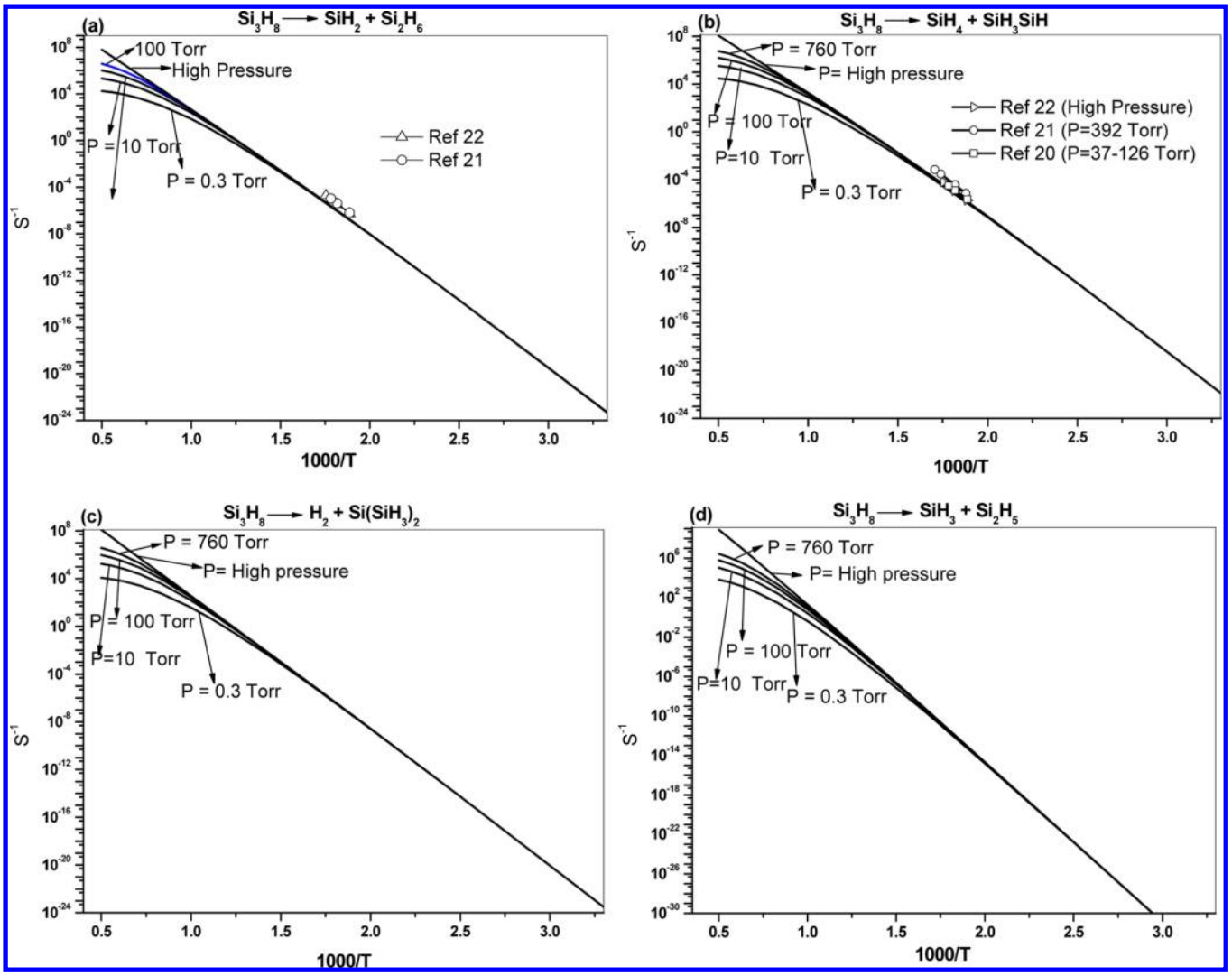

Figure 7. Arrhenius plots of rate constants for the Si_3H_8 unimolecular dissociation forming various products, $SiH_2 + Si_2H_6$ (a), $SiH_4 + SiH_3SiH$ (b), $H_2 + Si(SiH_3)_2$ (c), and $SiH_3 + Si_2H_5$ (d), at different pressures.

$\exp(229/T)$ cm^3 $molecule^{-1}$ s^{-1} for the temperature range of 295−595 K at 1.0−30.0 Torr in C_8H_8 buffer gas. At 500 K, our predicted rate 4.54×10^{-10} cm^3 $molecule^{-1}$ s^{-1} compares closely with the experimental rate 4.87×10^{-10} cm^3 $molecule^{-1}$ s^{-1}.[18,19] White et al.[15] theoretically estimated the rate constant at temperatures of 640−703 K with an order of magnitude lower value. At room temperature, the present predicted rate constants, 1.5×10^{-9} at 1 Torr and 1.9×10^{-9} at 10 Torr He pressure, are in reasonable agreement with the values of Inoue et al.,[16] 5.7×10^{-10} cm^3 $molecule^{-1}$ s^{-1}, in 1 Torr of He gas and those of Jasinski et al.[17] using laser absorption to obtain the 3.4×10^{-10} cm^3 $molecule^{-1}$ s^{-1} at 10 Torr in a He bath gas. When the pressure increases from 0.3 to 760 Torr, k_1 increases proportionally, as clearly illustrated in Figure 3a, reflecting the need for collisional deactivation of the excited Si_3H_8 adduct. Under low-pressure conditions, the reaction may yield Si_3H_8 fragmentation products such as $SiH_4 + SiH_3SiH$, $H_2 + Si(SiH_3)_2$//SiH_3SiH_2SiH, and $SiH_3 + Si_2H_5$; the predicted rate constants for all product channels in the 300−2000 K temperature range including the high- and low-pressure limits are shown in the Figure 3b−e. The pattern of the pressure dependencies of the rate constants for formation of the product pairs revealed by these figures reflects the competitive nature of the collisional deactivation versus fragmentation of the excited Si_3H_8. The calculated pressure-dependent rate constants for competing product formation at 500 K are displayed in Figure 4a. The results clearly show that the formation of Si_3H_8 by collisional deactivation is strongly *P*-dependent and dominant over the other production channels down to $P < 1$ Torr. The next dominant channel in the $SiH_2 + Si_2H_6$ reaction is $SiH_4 + SiH_3SiH$//Si_2H_4. Here, when the pressure increases, its rate also decreases due to the competition with Si_3H_8 formation. Figure 4b displays the branching ratios of the individual product channels of the $SiH_2 + Si_2H_6$ reaction at 1 Torr in the 300−2000 K temperature range. The results show that at 300 K, formation of Si_3H_8 is dominant with 99% yield, and the remaining 1% gives $SiH_4 + SiH_3SiH$. The production of Si_3H_8 up to 700 K temperature is dominant, above which $SiH_4 + SiH_3SiH$//Si_2H_4 becomes competitive. Other production channels are not important until reaching a higher temperature of 1700 K, at which $SiH_3 + Si_2H_5$ becomes competitive.

Rate Constant for $SiH_3 + Si_2H_5$. As aforementioned, the association reaction of SiH_3 with Si_2H_5 producing Si_3H_8 with more than 74.0 kcal/mol of internal energy occurs without a well-defined transition state; the Si_3H_8 thus formed can dissociate with 19 kcal/mol of excess energy above $SiH_2 + Si_2H_6$

dx.doi.org/10.1021/jp407553a | J. Phys. Chem. A 2013, 117, 10811−10823

Table 6. Arrhenius Parameters[a] for the Unimolecular Decomposition of Si_3H_8 Giving Different Products at Various Pressures and Temperatures Including High-Pressure (k_∞) and Low-Pressure (k_0) Limits

reaction	P (Torr)	A	n	E_a/R (K)	k_p(500 K)
$Si_3H_8 \rightarrow SiH_2 + Si_2H_6$ (k)	k_∞	7.64×10^{33}	−6.23	2887	9.89×10^{-9}
	k_0	3.70×10^{33}	−11.2	31263	1.60×10^{-24}
	0.3	1.07×10^{52}	−12.2	31263	9.28×10^{-9}
	1	5.70×10^{47}	−10.8	30736	9.66×10^{-9}
	10	2.64×10^{40}	−8.36	29774	9.86×10^{-9}
	760	2.43×10^{34}	−6.39	28942	9.89×10^{-9}
$Si_3H_8 \rightarrow SiH_4 + SiH_3SiH$ (k)	k_∞	8.59×10^{38}	−7.68	29126	8.24×10^{-8}
	k_0	5.87×10^{39}	−13.1	31567	1.18×10^{-23}
	0.3	1.70×10^{58}	−14.1	31567	6.81×10^{-8}
	1	4.52×10^{54}	−12.8	31182	7.63×10^{-8}
	10	1.66×10^{47}	−10.4	30255	8.16×10^{-8}
	760	4.87×10^{39}	−7.93	29231	8.24×10^{-8}
$Si_3H_8 \rightarrow H_2 + Si(SiH_3)_2$ (k)	k_∞	9.46×10^{22}	−2.83	27534	2.72×10^{-8}
	k_0	4.18×10^{26}	−9.1	30465	4.47×10^{-25}
	0.3	1.21×10^{45}	−10.1	30465	2.59×10^{-9}
	1	1.30×10^{40}	−8.4	29843	2.67×10^{-9}
	10	4.82×10^{31}	−5.66	28735	2.71×10^{-9}
	760	7.24×10^{23}	−3.12	27659	2.72×10^{-9}
$Si_3H_8 \rightarrow H_2 + SiH_3SiH_2SiH$	k_∞	8.86×10^{12}	0.09	26513	1.45×10^{-10}
	k_0	3.66×10^{11}	−4.48	28824	2.47×10^{-26}
	0.3	1.06×10^{30}	−5.48	28824	1.43×10^{-10}
	1	2.15×10^{25}	−3.94	28209	1.45×10^{-10}
	10	1.91×10^{18}	−1.64	27255	1.45×10^{-10}
	760	2.07×10^{13}	−0.03	26565	1.45×10^{-10}
$Si_3H_8 \rightarrow SiH_3 + Si_2H_5$	k_∞	2.02×10^{23}	−1.83	38031	2.14×10^{-15}
	k_0	8.68×10^{37}	−11.8	42161	2.73×10^{-31}
	0.3	2.51×10^{56}	−12.80	42161	1.58×10^{-15}
	1	1.79×10^{52}	−11.37	41734	1.81×10^{-15}
	10	1.90×10^{43}	−8.36	40683	2.06×10^{-15}
	760	5.86×10^{28}	−3.60	38787	2.13×10^{-15}

[a] $k(T) = AT^n \exp(-E_a/RT)$ predicted for various temperatures 300−1000 K in units of s^{-1} for k and k_∞ and cm^3 $molecule^{-1}$ $s^{-1}$for k_0.

and even higher above other product pairs; thus, various products, SiH_2, SiH_4, and H_2, can be formed from the association/decomposition reactions; see Figure 2 and reactions 6−10 presented in the Introduction section. The predicted values of k_6 forming Si_3H_8 at various pressures between 0.3 and 760 Torr along with its high-pressure limit in the temperature range of 300−2000 K are graphically presented in Figure 5a and are also listed in Table 5. In the table, the value for the low-pressure limit is also given for kinetic modeling. The values of k_6 decrease as the temperature increases from 300 to 2000 K. When the pressure increases from 0.3 to 760 Torr, k_6 increases proportionally, as clearly illustrated in Figure 5a, reflecting the effect of collisional deactivation of the excited Si_3H_8. The predicted rate constants for the $SiH_3 + Si_2H_5$ reaction giving rise to various products are shown in Figure 5b−e. The rate constants for production of Si_3H_8 (k_6) and various products (k_{7-10}) at 500 K covering the wide pressure range are shown in Figure 6a. The branching ratios of these five product channels are shown in Figure 6b. The product channel giving $SiH_4 + SiH_3SiH$ is predominant up to 1800 K. The competitive nature of reactions 6−10 shown in these figures is qualitatively similar to that presented above for reactions 1−5, as one would expect. The only difference between the two bimolecular reactions lies in the amount of internal energies carried by the chemically activated Si_3H_8*, as shown in the PES.

We have done the rate constant calculations for the forward reactions of $SiH_2 + Si_2H_6$ and $SiH_3 + Si_2H_5$, which form various products with and without multiple reflection corrections. At 300 K (the lowest temperature) and 760 Torr and the high-pressure limit, in the $SiH_2 + Si_2H_6 \rightarrow Si_3H_8$ reaction, the forward reaction rate constant with the multiple reflection correction is around 2 orders of magnitude lower than that without the correction. There is no effect of multiple reflection corrections above 700 K (see Supporting Information Figure S1A and B). At 300 K and 760 Torr, the multiple reflection correction for $SiH_2 + Si_2H_6 \rightarrow SiH_4 + SiH_3SiH$ (k_2) is around 1 order of magnitude lower than that without the correction, and no effect of correction is seen above 500 K (see Supporting Information Figure S1C). For other product channels of H_2 and SiH_3 (k_3, k_4, and k_5) in the above $SiH_2 + Si_2H_6$ reaction, the effect of the multiple reflection correction is negligible. For the forward reactions of $SiH_3 + Si_2H_5$ forming various low-energy product rate constants, we compared the results with and without multiple reflection corrections at 300 K and 760 Torr of pressure, as shown in Figure S2 (Supporting Information). In this case, no multiple reflection correction effect was observed.

Thermal Decomposition of Si_3H_8. The thermal decomposition of Si_3H_8 under similar conditions as those given above for the association process produces predominantly $SiH_4 + SiH_3SiH$ because of its lower-energy barrier compared with those for $SiH_2 + Si_2H_6$, H, and H_2 elimination from the primary and secondary positions. As shown in Figure 7 and the rate constant expressions summarized in Table 6 obtained by least-squares fitting to the predicted values, both reactions have

dx.doi.org/10.1021/jp407553a | J. Phys. Chem. A 2013, 117, 10811−10823

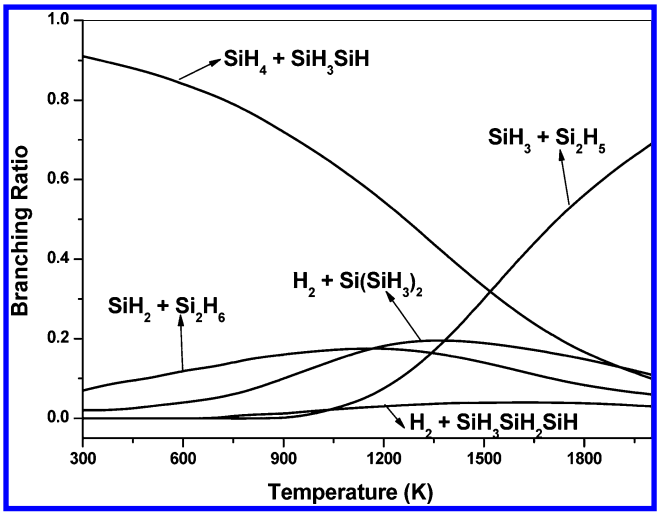

Figure 8. Branching ratios of Si_3H_8 decomposition products at high pressure.

positive-pressure dependence, reflecting the nature of collisional activation. Experimentally, Vanderwielen et al.[20] kinetically measured the unimolecular decomposition of Si_3H_8 to SiH_4 + SiH_3SiH and SiH_2 + Si_2H_6 in the 530−561 K temperature range and 37−126 Torr of Si_3H_8 pressure range. Later, Martin et al.[21] measured the rate constant for the decomposition pathways of Si_3H_8 → SiH_4 + SiH_3SiH by pyrolysis at 532−586 K and 392 Torr of H_2 pressure. In 1992, Moffat el al.[22] studied the rate constant for the decomposition channels of trisilane to form SiH_4 and SiH_2 products by RRKM numerial analysis in the temperature range of 530−570 K. The experimental results are in good agreement with our predicted values, as shown in Figure 7a and b.[20−22] The rate constants for other production channels by H_2 elimination from primary and secondary Si−H bonds are also shown in Figure 7c and d. Figure 8 shows the branching ratios of Si_3H_8 dissociation products; the low-energy channel producing SiH_4 + SiH_3SiH is dominant up to 1500 K, beyond which SiH_3 + Si_2H_5 becomes dominant. It should be pointed out that although the SiH_2 + Si_2H_6 product pair energetically lies below SiH_3 + Si_2H_5 by as much as 19 kcal/mol, its branching ratio was predicted to be less than that of the latter above 1300 K, attributable to the tighter transition state TS1 than the variational TS for the latter production.

CONCLUSION

The mechanisms, rate constants, and product branching ratios for the SiH_2 + Si_2H_6 and SiH_3 + Si_2H_5 reactions and the thermal unimolecular decomposition of Si_3H_8 have been investigated at the QCISD(T)/CBS level of theory based on QCISD/6-311++G(d,p) optimized geometries in conjunction with VTST and RRKM calculations. The formation of the most favorable low-energy products for the SiH_2 + Si_2H_6 reaction occurs readily by Si−H insertion, yielding the excited intermediate Si_3H_8 via the van der Waals complex with 8.3 kcal/mol of binding energy. The excited intermediate carrying as much as 55.0 kcal/mol of internal energy can readily dissociate into SiH_4 + SiH_3SiH// Si_2H_4 following the 2,1-H migration involving one of the H atoms in the secondary SiH_2 group. The excited intermediate can also decompose by H_2 elimination from the secondary position with 2.8 kcal/mol lower energy than that from the primary position, which requires 51.6 kcal/mol. The dissociation energies for breaking of the Si−Si and the primary and secondary Si−H bonds in Si_3H_8 were predicted to be 74.0, 85.0, and 86.9 kcal/mol, respectively. The values agree well with the known heats of formation of the decomposition products.

The computed heats of formation $\Delta_f H_0^\circ$ at 0 K for Si_3H_8, SiH_3, SiH_3SiH, Si_2H_4, *i*-Si_3H_7, *n*-Si_3H_7, $Si(SiH_3)_2$, and SiH_3SiH_2SiH are 33.5, 48.3, 77.3, 68.0, 66.9 ± 1.0, 68.7 ± 1.0, 87.1, and 87.3 kcal/mol, respectively, with an estimated error of ±1.2 kcal/mol. The results are in good agreement with available experimental values. Furthermore, the rate constants for the bimolecular association/decomposition reactions (SiH_2 + Si_2H_6 and SiH_3 + Si_2H_5) and the thermal unimolecular decomposition of Si_3H_8 for all of the product channels have been calculated using the VTST method and/or the RRKM theory by solving the master equation involved over a wide range of *P*,*T* conditions covering those typically employed in the a-Si/H CVD process by PECVD and/or Cat-CVD. The predicted results have been tabulated for modeling and optimizing homogeneous large-area growth of a-Si/H thin films by these methods.

ASSOCIATED CONTENT

Supporting Information

Calculated moments of inertia and vibrational frequencies of the species involved in the SiH_2 reactions with Si_2H_6 computed at the QCISD/6-311++G(d,p) level are given in Table S1, and Arrhenius plots of rate constants for the SiH_2 + Si_2H_6 and SiH_3 + Si_2H_5 reactions forming various products are given in Figures S1 and S2, respectively. This material is available free of charge via the Internet at http://pubs.acs.org.

AUTHOR INFORMATION

Corresponding Author

*E-mail: chemmcl@emory.edu.

Notes

The authors declare no competing financial interest.

ACKNOWLEDGMENTS

The authors deeply appreciate the support by Taiwan's National Science Council (NSC) under Contract No. NSC100-2113-M-009-013 and by the Ministry of Education's ATU program. M.C.L. also acknowledges the support from the NSC for the distinguished visiting professorship at National Chiao Tung University in Hsinchu, Taiwan. We are also grateful to the National Center for High-Performance Computing for computer time and the use of its facilities.

REFERENCES

(1) Gaspar, P. P. In *Silylenes, Reactive Intermediates*; Jones, M., Moss, Eds.; Wiley: New York, 1985; Vol. 3.

(2) Becerra, R.; Walsh, R. In *Research in Chemical Kinetics*; Compton, R.G., Hancock, G., Eds.; Elsevier: New York, 1995; Vol. 3, p 263.

(3) Jasinski, J. M.; Becerra,; Walsh, R. Direct Kinetic Studies of Silicon Hydride Radicals in the Gas Phase. *Chem. Rev.* **1995**, *95*, 1203−1228.

(4) Dietrich, T. R.; Chiussi, S.; Marek, M.; Roth, A.; Comes, F. J. Role of Sllylene in the Deposition of Hydrogenated Amorphous Silicon. *J. Phys. Chem.* **1991**, *95*, 9302−9310.

(5) Jasinski, J. M.; Whittaker, E. A.; Bjorklund, G. C.; Dreyfus, R. W.; Estes, R. D.; Walkup, R. E. Detection of SiH_2 in Silane and Disilane Glow Discharges by Frequency Modulation Absorption Spectroscopy. *Appl. Phys. Lett.* **1984**, *44*, 1155−1157.

(6) Jasinski, J. M.; Gates, S. M. Silicon Chemical Vapor Deposition One Step at a Time: Fundamental Studies of Silicon Hydride Chemistry. *Acc. Chem. Res.* **1991**, *24*, 9−15.

(7) Lecomber, P. G.; Spear, W. E; Ghaith, A. Amorphous-Silicon Field-Effect Device and Possible Application. *Electron. Lett.* **1979**, *15*, 179−181.
(8) Carlson, D. E.; Wronski, C. R. Amorphous Silicon Solar Cell. *Appl. Phys. Lett.* **1976**, *28*, 671−673.
(9) Kushner, M. J. A Model for the Discharge Kinetics and plasma Chemistry During Plasma Enhanced Chemical Vapor Deposition of Amorphorous Silicon. *J. Chem. Phys.* **1988**, *63*, 2532−2551.
(10) Matsuda, A. Thin-Film Silicon — Growth Process and Solar Cell Application. *Jpn. J. Appl. Phys.* **2004**, *43*, 7909−7920.
(11) Matsumura, H. Formation of Silicon-Based Thin Films Prepared by Catalytic Chemical Vapor Deposition (Cat-CVD) Method. *Jpn. J. Appl. Phys.* **1998**, *37*, 3175−3187.
(12) Matsumura, H.; Umemoto, H.; Masuda, A. Cat-CVD (Hot-Wire CVD): How Different from PECVD in Preparing Amorphous Silicon. *J. Non-Cryst. Solids* **2004**, *338*−*340*, 19−26.
(13) Roth, A.; Chiussi, S.; Dietrich, T. R.; Comes, F. J. Hydrogenated Amorphous Silicon by Infrared Multiphoton Absorption with a Pulsed CO_2-Laser. *Ber. Bunsen-Ges. Phys. Chem* **1990**, *94*, 1105−1110.
(14) John, P.; Purnell, J. H. Arrhenius Parameters for Silene Insertion Reactions. *J. Chem. Soc., Faraday Trans. 1* **1973**, *69*, 1455−1461.
(15) White, R. T.; Espino-Rios, R. L.; Rogers, D. S.; Ring, M. A.; O'Neal, H. E. Mechanism of the Silane Decomposition. I. Silane Loss Kinetics and Rate Inhibition by Hydrogen. II. Modeling of the Silane Decomposition (All Stages of Reaction). *Int. J. Chem. Kinet.* **1985**, *17*, 1029−1065.
(16) Inoue, G.; Suzuki, M. Reactions of $SiH_2(X^1A_1)$ with H_2, CH_4, C_2H_4, SiH_4 and Si_2H_6 at 298 K. *Chem. Phys. Lett.* **1985**, *122*, 361−364.
(17) Jasinski, J. M.; Chu, J. O. Absolute Rate Constants for the Reaction of Silylene With Hydrogen, Silane, and Disilane. *J. Chem. Phys.* **1988**, *88*, 1678−1687.
(18) Baggott, J. E.; Frey, H. M.; Lightfoot, P. D.; Walsh, R.; Watts, I. M. Absolute Rate Constants for the Gas-Phase Reactions of Silylene with Silane, Disilane and the Methylsilanes. *J. Chem. Soc., Faraday Trans. 1* **1990**, *86*, 27−33.
(19) Becerra, R.; Frey, H. M.; Manson, B. P.; Walsh, R. Time-Resolved Gas-Phase Kinetic Studies of the Reactions of Silylene with Disilane and Trisilane. *J. Organomet. Chem.* **1996**, *521*, 343−349.
(20) Vanderwielen, A. J.; Ring, M. A.; O'Neal, H. E. Kinetics of the Thermal Decomposition of Methyldisilane and Trisilane. *J. Am. Chem. Soc.* **1975**, *97*, 993.
(21) Martin, J. G.; O'Neal, H. E; Ring, M. A. Thermal Decomposition Kinetics of Polysilanes: Disilane, Trisilane, and Tetrasilane. *Int. J. Chem. Kinet.* **1990**, *22*, 613−632.
(22) Moffat, H. K.; Jensen, K. F.; Carr, R. W. J. Estimation of Arrhenius Parameters for the 1,l Elimination of H, from Si_2H_6 and the Role of Chemically Activated Disilane in Silane Pyrolysis. *J. Phys. Chem.* **1992**, *96*, 7695−7703.
(23) Kumata, K.; Itah, U.; Toyoshima, Y.; Tanaka, N.; Anzai, H.; Matsuda, A. Photochemical Vapor Deposition of Hydrogenated Amorphous Silicon Films from Disilane and Trisilane Using a Low Pressure Mercury Lamp. *Appl. Phys. Lett.* **1986**, *48*, 1380−1382.
(24) Kanoh, H.; Sugiura, O.; Matsumura, M. Chemical Vapor Deposition of Amorphous Silicon Using Tetrasilane. *Jpn. J. Appl. Phys.* **1993**, *32*, 2613−2619.
(25) Wu, S. Y.; Raghunath, P.; Wu, S. J.; Lin, M. C. Ab Initio Chemical Kinetic Study for Reactions of H Atoms with SiH_4 and Si_2H_6: Comparison of Theory and Experiment. *J. Phys. Chem. A* **2010**, *114*, 633−639.
(26) Varma, D. H.; Raghunath, P.; Lin, M. C. Ab Initio Chemical Kinetics for the Reaction of an H Atom with Si_3H_8. *J. Phys. Chem. A* **2010**, *114*, 3642−3648.
(27) Raghunath, P.; Lin, M. C. Ab Initio Chemical Kinetics for SiH_3 Reactions with Si_xH_{2x+2} (x = 1−4). *J. Phys. Chem. A* **2010**, *114*, 13353−13361.
(28) Raghunath, P.; Lee, Y. M.; Wu, S. Y.; Wu, S. J.; Lin, M. C. Ab Initio Chemical Kinetics for Reactions of H Atoms with SiH_x (x = 1−3) Radicals and Related Unimolecular Decomposition Processes. *Int. J. Quantum. Chem.* **2013**, *113*, 1735−1746.
(29) Pople, J. A.; Head-Gordon, M.; Raghavachari, K. Quadratic Configuration Interaction. A General Technique for Determining Electron Correlation Energies. *J. Chem. Phys.* **1987**, *87*, 5968−5975.
(30) Matsumoto, K.; Klippenstein, S. J.; Tonokura, K.; Koshi, M. Channel Specific Rate Constants Relevant to the Thermal Decomposition of Disilane. *J. Phys. Chem. A* **2005**, *109*, 4911−4920.
(31) Pei, K.; Li, H. Ab Initio and Kinetic Calculations for the Reactions of Cl with SiH_nCl_{4-n}(n=1−4). *J. Chem. Phys.* **2004**, *121*, 6738−6742.
(32) Peterson, K. A.; Woon, D. E.; Dunning, T. H., Jr. Benchmark Calculations with Correlated Molecular Wave Functions. IV. The Classical Barrier Height of the H + H_2 → H_2 + H Reaction. *J. Chem. Phys.* **1994**, *100*, 7410−7415.
(33) Woon, D. E., Jr.; Dunning, T. H. Gaussian Basis Sets for Use in Correlated Molecular Calculations. V. Core-Valence Basis Sets for Boron through Neon. *J. Chem. Phys.* **1995**, *103*, 4572−4585.
(34) Frisch., M. J.; Trucks, G. W.; Schlgel, H. B.; Scuseria, G. E.; Robb, M. A. Cheeseman, J. R.; Iyengar, S. S.; Tomasi, J.; Barone, V.; Mennucci, B.; et al. *Gaussian 03*, revision C.02; Gaussian, Inc.: Wallingford, CT, 2004.
(35) Klippenstein, S. J.; Wagner, A. F.; Dunbar, R. C.; Wardlaw, D. M.; Robertson, S. H. *VARIFLEX*, version 1.00; Argonne National Laboratory: Argonne, IL, USA, 1999.
(36) Klippenstein, S. J. An Efficient Procedure for Evaluating the Number of Available States within a Variably Defined Reaction Coordinate Framework. *J. Phys. Chem.* **1994**, *98*, 11459−11464.
(37) Klippenstein, S. J. A Bond length Reaction Coordinate for Unimolecular Reactions. II. Microcanonical and Canonical Implementations with Application to the Dissociation of NCNO. *J. Chem. Phys.* **1991**, *94*, 6469−6482.
(38) Werner, H.-J.; Knowles, P. J., with contributions from Almlof, J.; Amos, R. D.; Berning, A.; et al. *MOLPRO*, version 2009.1, a Package of ab initio programs; University College Cardiff Consultants Limited: Cardiff, U.K., 2009.
(39) Callomnon, J. H.; Hirota, E.; Kuchitsu, K.; Lafferty, W. J.; Maki, A. G. ; Pote, C. S. *Structure Data on Free Polyatomic Molecules (Landolt-Bornstein, New Series, Group 11)*; Springer-Verlag: Berlin, Germany, 1976, Vol. 7.
(40) Haaland, A.; Rypdal, K.; Stuger, H.; Volden, H. V. Molecular-Structures and Conformational Composition of Trisilane by Gas-Phase Electron-Diffraction. *Acta Chem. Scand.* **1994**, *48*, 46−51.
(41) Katzer, G.; Ernst, M. C.; Sax, A. F.; Kalcher, J. Computational Thermochemistry of Medium-Sized Silicon Hydrides. *J. Phys. Chem. A* **1997**, *101*, 3942−3958.
(42) Chase, M. W. Jr. NIST-JANAF Thermochemical Tables, 4th ed., *J. Phys. Chem. Ref. Data* **1998**; Monograph No. 9 (Parts I and II).
(43) Rustic, B.; Berkowitz, J. Photoionization Mass Spectrometric Studies of the Transient Species Si_2H_n (n=2−5). *J. Chem. Phys.* **1991**, *95*, 2416−2432.
(44) Miller, W. H. Unified Statistical Model for "Complex" and "Direct" Reaction Mechanisms. *J. Chem. Phys.* **1976**, *65*, 2216−2223.
(45) Chakraborthy, D.; Hsu, C.-C.; Lin, M. C. Theoretical Studies of Nitroamino Radical Reactions: Rate Constants for the Unimolecular Decomposition of $HNNO_2$ and Related Bimolecular Processes. *J. Chem. Phys.* **1998**, *109*, 8887−8896.
(46) Xu, Z. F.; Hsu, C. -H.; Lin, M. C. Ab Initio Kinetics of the Reaction of HCO with NO: Abstraction versus Association/Elimination Mechanism. *J. Chem. Phys.* **2005**, *122*, 234308/1−234308/11.
(47) Coltrin, M. E.; Kee, R. J.; Miller, J. A. A Mathematical Model of Silicon Chemical Vapor Deposition. *J. Electrochem. Soc.* **1986**, *133*, 1206−1213.